International Journal of Engineering & Technology, 7 (4.39) (2018) 330-334

International Journal of Engineering & Technology

Website: www.sciencepubco.com/index.php/IJET

Research paper

Phase Field Modeling of Coalescence of AlSi10Mg Particles in Direct Metal Laser Sintering

Jyotirmoy Nandy[1]*, Seshadev Sahoo[2], Hrushikesh Sarangi[3], Bibhu Kalyan Panda[4]

[1]*Department of Mechanical Engineering, Institute of Technical Education and Research, Siksha 'O' Anusandhan, Odisha, India*
**Corresponding author E-mail: jyotirmoynanday@soa.ac.in*

Abstract

Direct metal laser sintering (DMLS) is amongst the most proficient technologies in the field of additive manufacturing which produces high quality products. The physical properties of the final products is immensely affected by the process parameters of the process. Being a fast process, the solidification rate is very fast as powdered materials sinter into crystalline structures with the application of laser power. Since the past few decades, computational modeling has helped researchers to predict and optimize the quality of output products. In this study, phase field modeling has been used to study the sintering mechanism and importance of neck growth of AlSi10Mg in DMLS process. Using temperature as an input parameter to study neck growth in equal and unequal sized particles, it is found that the rise in temperature leads to higher neck growth. It has been found that unequal sized particles experience faster sintering due to high diffusion rate. Also, by increasing the laser power, it has been found that the sintering rate is faster.

Keywords: *Direct metal laser sintering; coalescence; additive manufacturing; phase field modeling*.

1. Introduction

Sintering is an old process which includes the compaction of powdered alloys or pure metals using heat and pressure. Due to complications in processing and defects in the final products, the direct metal laser sintering (DMLS) is gaining popularity and is further proving to be more efficient in the recent times. Being a part of additive manufacturing, the process works on the principle of the layer-by-layer build technique. A very high powered laser beam is used for scanning the geometry of the required shape and sinters/compacts the powdered materials. The schematic diagram of DMLS process is shown in Figure 1. It is a rapid solidification process and consists of two parts mainly-solid state sintering and liquid state sintering. The solid state sintering is caused mainly by mass diffusion and plastic flow. In the liquid state sintering, other additives which have lower melting points are added to increase strength by liquefying as binders. Howsoever the process parameters of the DMLS process control the thermal and mechanical properties of the final outputs [1-4]. Hence the study of microstructure is becoming very important in the development and understanding of new alloys. Out of many new alloys, AlSi10Mg has found its usage in varied fields such as aerospace, biomechanical and automobile. High strength, good hardenability and low cost of makes AlSi10Mg highly preferable for making parts which are subjected to very high loads [5-7]. During the DMLS process, many intricate phenomenon take place such as diffusion, mass flow and solidification. Out of the above three, diffusion helps in determining the actual microstructure of the resultant output. Grain boundary diffusion, surface diffusion, volume bulk diffusion and vapour diffusion are the essential entities of the overall diffusion process. To analyze the changes occurred during these , a microstructural model is very much needed. The early prediction and control over these parameters can provide an upper hand to the researchers all over the world.

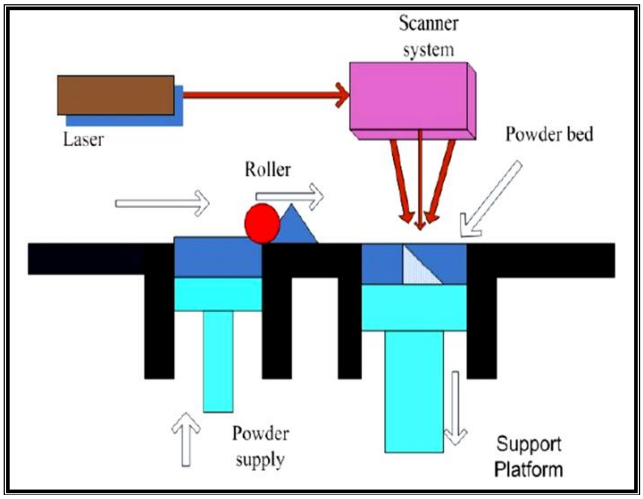

Fig. 1: Schematic diagram of DMLS

In the past few decades, computational modeling has been carried out in different length and time scales. Rigorous developments has been made in developing new computational tools which have further helped reducing the computational time and increase efficiency. Also, many efforts have been made in modeling the sintering process. Continuum [8, 9] and atomistic models [10-12] have been used by researchers throughout the world to study the sintering behavior of various metals and alloys. Out of all the above, phase field modeling has proved to be an efficient tool in modeling microstructures at the mesoscopic level. The feasibility of tracking of particles at the interfacial region in phase field modeling is an advantage over many other continuum models [13].

Till date, no such study has been reported which studies the necking and coalescence of laser sintered AlSi10Mg at different laser powers using phase field modeling. Hence, in this paper a phase field model is built up to study the necking and coalescence of AlSi10Mg by analyzing the neck growth and dihedral angle of equal as well as unequal sized particles.

2. Literature Review

R.E Mistler et al. [14] developed a method for calculating the width of the grain-boundary and grain-boundary diffusion coefficients in metals and non-metals using different quantitative data like grain growth, sintering, and diffusion data. D Lynn Johnson et al. [15] developed a sintering model in which they proposed all of the noteworthy mechanisms of material transport and identified that each mechanism operates simultaneously. Nandy et al. [16] carried out phase field simulations using AlSi10Mg in DMLS to study the dendritic tip growth in single as well as multi-particle arrangements. The simulations were carried out using temperature gradient as an input parameter. Wang et al. [17] stated that LED has a significant effect on surface morphology of the built form part that is higher LED might advance to the balling phenomena, whilst small LED would lead to production of defects like porosity and micro crack which leads to porosities and affect surface roughness. C.A Biffi et al. [18] evaluated and studied the mechanical tests that were carried on AlSi10Mg samples made by selective laser melting technique in X-Y building alignment. A similar composition was achieved. Noaki Takata et al. [19] carried studies on variation of microstructure and mechanical properties of the AlSi10Mg alloy, it absolutely was seen that once producing mistreatment selective optical maser melting (SLM) combined with a multi-particle bed system, by application of heat at temperatures of every three hundred or 530 °C. Yuchao Bai et al. [20] investigated the consequence of selective optical maser melting method properties on comparative densification parameters of AlSiMg0.75 alloy with flat and square samples that were made-up with optimized method parameters, to review the tensile, small hardness and microstructure evolution.

3. Model Formulation using Phase Field Method

A phase field model is developed using two field variables-conserved field variable and non-conserved field variable. Density field (ρ) is taken as the conserved field variable which attains a quantitative value of 1 at the solid region and 0 value at the pore surface. In this model, a rapid change in the solid-pore interfacial region is assumed. The non-conserved order parameter, 'ηi' is a parameter which distinguishes various particles at the interface and microstructure.

The free energy function [21] of the field variables in the microstructure evolution is described as follows,

$$F = \int_v \left[(\rho, \eta_{1....p}) + \frac{K_\rho}{2}(\nabla_\rho)^2 + \sum_i \frac{K_\eta}{2}(\nabla \eta_i)^2 \right] dv \quad (1)$$

In which,

K_ρ=concentration coefficient of gradient energy,

K_η= Parameter for Grain boundary energy

The evolution of energy density function, ρ which is a conserved parameter can be defined according to the Cahn-Hilliard [22] equation as,

$$\frac{\partial \rho}{\partial t} = \nabla . D \nabla \left(\frac{\partial f}{\partial \rho} - K_\rho \nabla^2 \rho \right) \quad (2)$$

The evolution of non-conserved parameters, η_i which distinguishes the different particles can be defined according to the Allen-Cahn [23] equation as,

$$\frac{\partial \eta_i}{\partial t} = -L\left(\frac{\partial f}{\partial \eta_i} - K_\eta \nabla^2 \eta_i \right) \quad (3)$$

Where,

L= grain boundary mobility

The microstructure dependent diffusivity [24], D can be calculated as,

$$D = D_{vol}\phi(\rho) + D_{vap}[1-\phi(\rho)] + D_{surf}\rho(1-\rho) + D_{GB}\sum_i \sum \eta_i \eta_m \quad (4)$$

Here,

D_{vol}= Bulk diffusion coefficient,

D_{vap}= Vapour diffusion coefficient,

D_{surf}= Surface diffusion coefficient &

D_{GB}= Grain boundary diffusion coefficient

Equation 4 tracks the interfacial region and the grain boundaries with respect to the different diffusion mechanisms mentioned above.

4. Assumptions and Approach for Phase Field Simulation

The phase field simulations are carried out using temperatures from a thermal model elsewhere [25]. These temperatures are inserted in the code using the mobility parameter. A five-point stencil in 2-D space is created using the finite difference methodology for solving the principal equations. Mainly, approximation method is adopted for the Laplacian operator and the dimensional derivatives. Time integration is sorted using the Euler marching format for time. MATLAB is used as a platform for performing the simulations and solving the equations of phase field model. The top surface of the powder bed is taken into consideration in this paper where the built-up geometry is kept at X and Y direction. In both directions, the domain size is set at 100μm each. The domain is further divided into grids of 100x100 for both equal and unequal sized particles and the grid spacing is set at dx=dy=0.5μm. Initially the simulation domain is set using two circular seeds of diameter 20μm each for equal sized particles and 20μm-10μm for the pair of unequal sized particles. The laser power is set at 70W for first set and 100W for second set of simulations. The scan speed is kept constant at 100mm/s.

The simulations are carried in MATLAB using the following procedure:

a) The preliminary parameters of the model have been outlined and phase field variables are calculated in the simulation area.
b) The material related parameters are set and order parameters are enabled in the code for the microstructure modeling.
c) For each and every grid point, the free energy of concentration field is obtained and accumulated in a function along with constant boundary conditions.
d) At all grid points, the mobility field is activated and calculated with integration of time.
e) Using the finite difference scheme and MATLAB the phase field equations are solved.
f) Periodic boundary conditions are set and temperature values are inserted according to the diffusion coefficients.

New values are then inserted to update the parameters and steps (c) and (d) are repeated for new iterations till the phase field is at boundary.

5. Results and Discussion

5.1 Sintering of Equal and Unequal Sized Particles

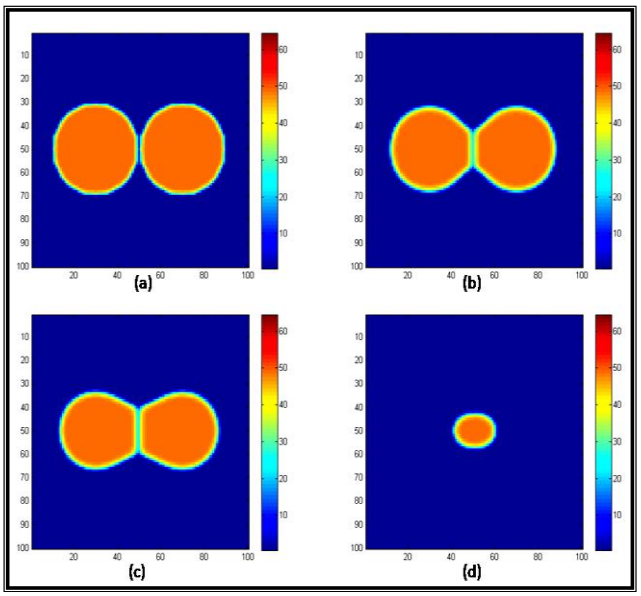

Fig. 2: Phase profile of equal sized AlSi10Mg particles at different times for laser power 70W (a) t=0s (b) t=25000ms (c) t=50000ms (d) t=60000ms

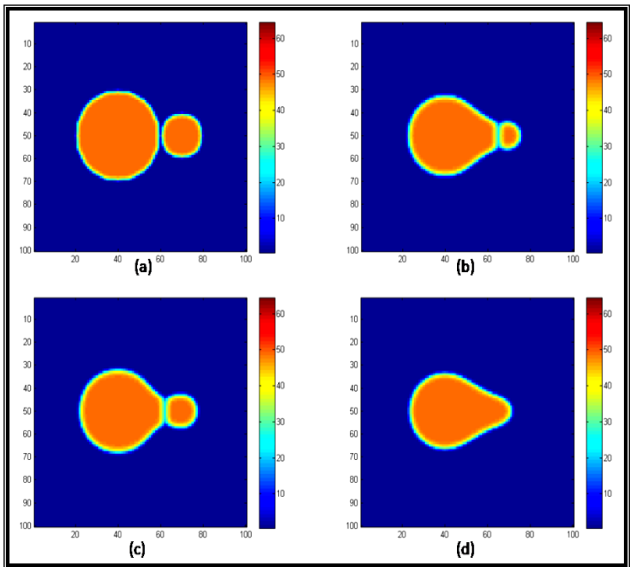

Fig. 3: Phase profile of unequal sized AlSi10Mg particles at different times for laser power 70W (a) t=0ms (b) t=10000ms (c) t=25000ms (d) t=50000s

Figure 2 and 3 shows the phase profiles of laser sintered AlSi10Mg for equal and unequal sized particles respectively at laser power 70W. At different times, the profiles show the initiation of necking, sintering and coalescence. In equal sized particles, the necking is prominent at 25000ms as shown in Fig. 2(b). The grain boundary diffusion starts causes the initial necking whereas the surface diffusion causes the necking to expand till t=50000ms (Fig. 2(c)). As the surface energy is lost, the volume bulk diffusion takes place which causes the coalescence of the equal sized particles at t=60000ms. It can be clearly seen from Fig. 2(d) that he particles have merged completely to become a single particle. For unequal sized particles, the grain boundary diffusion starts the initial necking and it can be seen from Fig. 3(b) that the necking starts faster at t=10000ms for unequal sized particles. At t=25000ms, most of necking takes place as observed in Fig. 3(c). The coalescence completes at t=50000ms for unequal sized particles. The smaller particle has smaller surface area in the system due to which it loses its internal energy faster than the previous system. As a result of this, the larger particle engulfs the smaller particle faster. Hence in case of unequal sized particles, sintering is faster due to faster grain boundary, surface and volume bulk diffusion.

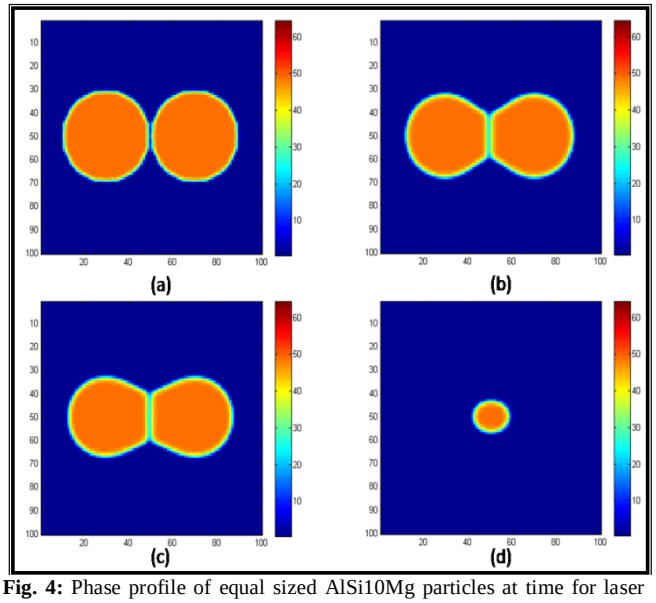

Fig. 4: Phase profile of equal sized AlSi10Mg particles at time for laser power 100W (a) t=0s (b) t=20000ms (c) t=50000ms (d) t=55000ms

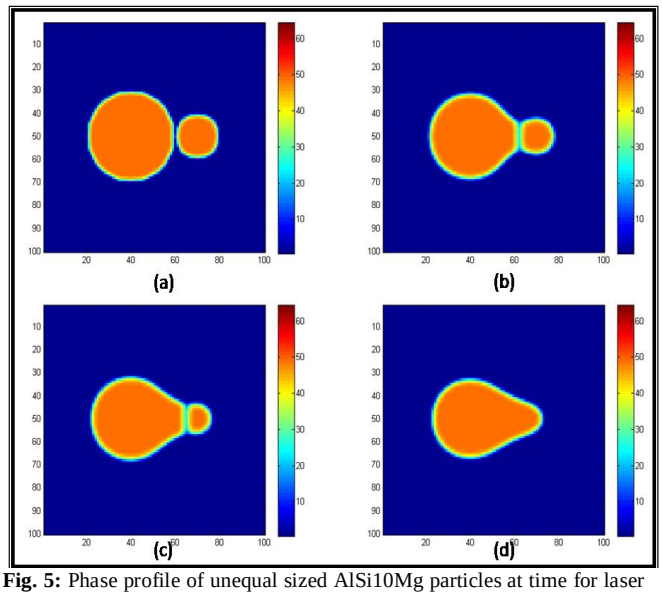

Fig. 5: Phase profile of unequal sized AlSi10Mg particles at time for laser power 100W (a) t=0s (b) t=5000ms (c) t=20000ms (d) t=40000ms

Figure 4 and 5 shows the phase profiles of laser sintered AlSi10Mg for equal and unequal sized particles respectively at laser power 100W. At different times, the profiles show the initiation of necking, sintering and coalescence. In equal sized particles, the necking is faster as that compared to 70W and is prominent at 25000ms as shown in Fig. 4(b). The grain boundary diffusion starts early in this case which causes the preliminary necking. In this case, surface diffusion causes the necking to expand till t=50000ms (Fig. 4(c)). Due to loss in surface energy, the volume bulk diffusion causes the coalescence of the equal sized particles earlier at t=55000ms. It can be clearly seen from Fig. 4(d) that there is formation of a single particle. In case of unequal sized particles at 100W laser power, the grain boundary diffusion starts the necking and it can be seen from Fig. 5(b) that the necking starts faster than that in 70W case (t=5000ms). At t=20000ms, it can be observed that maximum amount necking takes place as observed in Fig. 5(c). The coalescence is complete at t=40000ms

for laser power 100W (Fig. 5(d)). The increase in laser power from 70W to 100W causes faster sintering and is clearly visible by the measurement of neck width. As a result of this, this can be concluded that with higher laser power, the diffusion rate is higher which causes sintering to complete at a earlier stage.

5.2 Necking Analysis and Comparison between Equal and Unequal Sized Particles at Different Laser Powers

Figure 6 shows the geometry of necking phenomena. 'G' is the particle diameter and the distance between particle centre can be seen as 'δ'. 'X' is the neck width which can be measured theoretically using dihedral angle 'θ' as follows [26]:

$$X = G\sin\left(\frac{\theta}{2}\right) \tag{5}$$

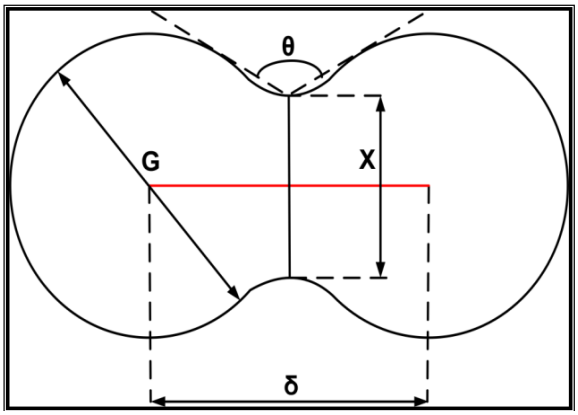

Fig.6: Geometry of neck width

At t=50000ms, the dihedral angle is measured for both equal and unequal sized particles. For equal sized particles, the dihedral angle is found to be 127.75° and for unequal sized particles it is found to be 122.05°. From Eq. 5, the calculated neck width has been measured to be 17.95μm for equally sized particles. The same has been measured to be 8.61μm for unequally sized particles. The neck width is also measured from the phase profiles for both equal and unequal sized particles which are found to be 18.01μm and 8.75μm respectively. The measured values are in good agreement with the calculated values.

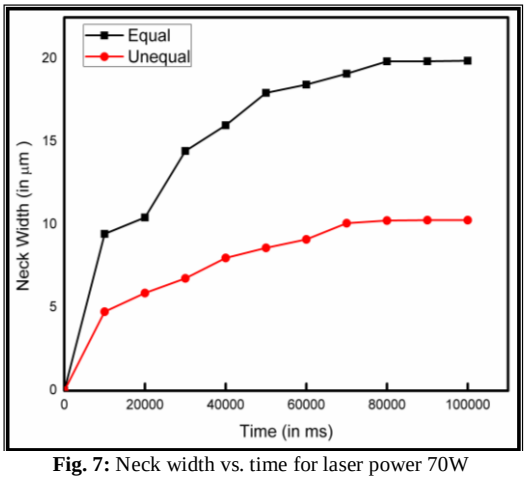

Fig. 7: Neck width vs. time for laser power 70W

From Fig. 7, it can be observed that, in equal sized particles with increase in time, there is increase of neck width. This is a result of the driving forces from both sides of the particles which is equal as both the particles are of same size. Also, as the sintering proceeds it decreases due to particle-shrinkage and volume diffusion apparently is more than other diffusion processes. Similarly, for unequal sized particles, the neck width follows the same trend as shown in Fig. 7. With the increase in laser power as well as sintering time, the neck width peaks appear. As compared to the equal sized particles, the neck width is lesser quantitatively due to the smaller surface area of one of the particles. The surface diffusion is higher in this case and the larger particle tends to engulf the smaller one which further causes a sudden transition in the graph. This analysis shows that diffusion rate in unequal sized particles is much higher than that in equal sized particles.

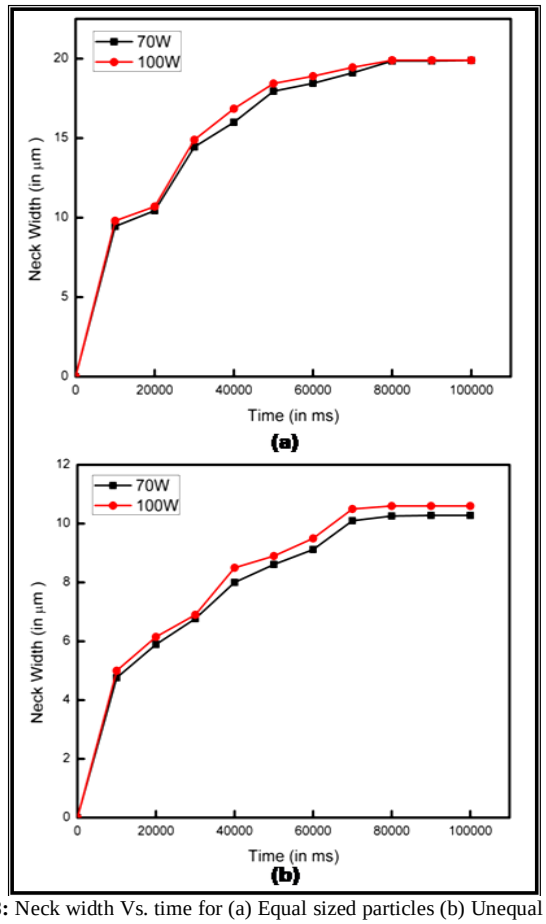

Fig. 8: Neck width Vs. time for (a) Equal sized particles (b) Unequal sized particles

Figure 8 shows the comparison between neck width of equal and unequal sized particles for 70W and 100W. For equal sized particles it can be seen from Fig. 8(a) that the neck width is larger for the same sintering time for laser power 100W. As compared to a neck width of 17.95μm in 70W case, the neck width is 18.44μm in case of laser power 100W. Similarly in case of unequal sized particles, the increase in laser power increases the sintering rate and in very less amount of time the final sintering condition is achieved. As the neck width is calculated for unequal sized particles at both 70W and 100W cases, it is found to be 6.15μm for 100W laser power, which is greater than that in case of 70W (5.89μm).

6. Conclusion

The necking behavior and sintering mechanism of AlSi10Mg is studied at laser power 70W for the DMLS process using a phase field model. The set of governing phase field equations for both equal and unequal sized particles using a MATLAB code. Temperature is integrated in the mobility function of the phase field model which is further extracted from a thermal model of the same process. From the results, it can be concluded that unequal particles require lesser sintering time to coagulate as the rate of

sintering is higher. Also, from the neck growth analysis, it can be concluded that the diffusion rate is faster in unequal sized particles as surface diffusion plays a vital role in complete coalescence of the particles. It can also be seen that by increasing the laser power, necking occurs faster in both equal and unequal sized particles.

References

[1] Gåård, A., Krakhmalev, P. and Bergström, J. (2006) 'Microstructural characterization and wear behavior of (Fe, Ni)–TiC MMC prepared by DMLS', Journal of Alloys and Compounds, Vol. 421, No. 1-2, pp.166-171.

[2] Calignano, F., Manfredi, D., Ambrosio, E.P., Iuliano, L. and Fino, P. (2013) 'Influence of process parameters on surface roughness of aluminum parts produced by DMLS', The International Journal of Advanced Manufacturing Technology, Vol. 67, No. 9-12, pp.2743-2751.

[3] Shellabear, M. and Nyrhilä, O. (2004) 'DMLS-Development history and state of the art', Laser Assisted Netshape Engineering 4, Proceedings of the 4th LANE, pp.21-24.

[4] Nandy, J., Sarangi, H. and Sahoo, S. (2017) 'February. Modeling of microstructure evolution in direct metal laser sintering: A phase field approach', In IOP Conference Series: Materials Science and Engineering, Vol. 178, No. 1, p. 012028.

[5] Krishnan, M., Atzeni, E., Canali, R., Calignano, F., Manfredi, D., Ambrosio, E. P., & Iuliano, L. (2014) 'On the effect of process parameters on properties of AlSi10Mg parts produced by DMLS', Rapid Prototyping Journal, Vol. 20, No. 6, pp.449-458.

[6] Fulcher, Benjamin A., David K. Leigh, and Trevor J. Watt (2014) 'Comparison of AlSi10Mg and Al 6061 processed through DMLS', Proceedings of the Solid Freeform Fabrication (SFF) Symposium, Vol. 46.

[7] Atzeni, E., & Salmi, A. (2015) 'Study on unsupported overhangs of AlSi10Mg parts processed by Direct Metal Laser Sintering (DMLS)', Journal of Manufacturing Processes, Vol. 20, No. 3, pp.500-506.

[8] Jagota, A., Dawson, P.R. and Jenkins, J.T. (1988), 'An anisotropic continuum model for the sintering and compaction of powder packings', Mechanics of Materials, Vol. 7, No.3, pp.255-269.

[9] Braginsky, M., Tikare, V. and Olevsky, E. (2005) 'Numerical simulation of solid state sintering', International journal of solids and structures, Vol. 42, No. 2, pp.621-636.

[10] Thomas, D.A., Lin, Z., Zhigilei, L.V., Gurevich, E.L., Kittel, S. and Hergenröder, R. (2009) 'Atomistic modeling of femtosecond laser-induced melting and atomic mixing in Au film–Cu substrate system', Applied Surface Science, Vol. 255, No. 24, pp.9605-9612.

[11] Yang, L., Gan, Y., Zhang, Y. and Chen, J.K. (2012) 'Molecular dynamics simulation of neck growth in laser sintering of different-sized gold nanoparticles under different heating rates', Applied Physics A, Vol. 106, No. 3, pp.725-735.

[12] Jiang, S., Zhang, Y., Gan, Y., Chen, Z. and Peng, H. (2013) 'Molecular dynamics study of neck growth in laser sintering of hollow silver nanoparticles with different heating rates', Journal of Physics D: Applied Physics, Vol. 46, No. 33, p.335302.

[13] Karma, A. and Rappel, W.J. (1996) 'Phase-field method for computationally efficient modeling of solidification with arbitrary interface kinetics', Physical Review E, Vol. 53, No. 4, p.R3017.

[14] Mistler, R.E. and Coble, R.L. (1974) 'Grain-boundary diffusion and boundary widths in metals and ceramics', Journal of Applied Physics, Vol. 45, No. 4, pp.1507-1509.

[15] Johnson, D.L. (1969) 'New Method of Obtaining Volume, Grain-Boundary, and Surface Diffusion Coefficients from Sintering Data', Journal of Applied Physics, Vol. 40, No. 1, pp.192-200.

[16] Nandy, J., Sarangi, H. and Sahoo, S. (2018) ' Microstructure evolution of Al-Si-10Mg in direct metal laser sintering using phase-field modeling', Advances in Manufacturing, Vol. 6, No. 1, pp.107-117.

[17] Wang, L.Z., Wang, S. and Wu, J.J. (2017) 'Experimental investigation on densification behavior and surface roughness of AlSi10Mg powders produced by selective laser melting', Optics & Laser Technology, Vol. 96, pp.88-96.

[18] Biffi, C.A., Fiocchi, J., Bassani, P., Paolino, D.S., Tridello, A., Chiandussi, G., Rossetto, M. and Tuissi, A. (2017) 'Microstructure and preliminary fatigue analysis on AlSi10Mg samples manufactured by SLM', Procedia Structural Integrity, Vol. 7, pp.50-57.

[19] Takata, N., Kodaira, H., Sekizawa, K., Suzuki, A. and Kobashi, M. (2017) 'Change in microstructure of selectively laser melted AlSi10Mg alloy with heat treatments', Materials Science and Engineering: A, Vol. 704, pp.218-228.

[20] Bai, Y., Yang, Y., Xiao, Z., Zhang, M. and Wang, D. (2018) 'Process optimization and mechanical property evolution of AlSiMg0. 75 by selective laser melting', Materials & Design, Vol. 140, pp.257-266.

[21] Steinbach, I., Pezzolla, F., Nestler, B., Seeßelberg, M., Prieler, R., Schmitz, G.J. and Rezende, J.L. (1996) 'A phase field concept for multiphase systems. Physica D: Nonlinear Phenomena', Vol. 94, No. 3, pp.135-147.

[22] Cahn, J.W., Elliott, C.M. and Novick-Cohen, A. (1996) 'The Cahn–Hilliard equation with a concentration dependent mobility: motion by minus the Laplacian of the mean curvature', European journal of applied mathematics, Vol. 7. No. 3, pp.287-301.

[23] Zhang, J. and Du, Q. (2009) 'Numerical studies of discrete approximations to the Allen–Cahn equation in the sharp interface limit', SIAM Journal on Scientific Computing, Vol. 31, No. 4, pp.3042-3063.

[24] Biswas, S., Schwen, D., Singh, J. and Tomar, V. (2016) 'A study of the evolution of microstructure and consolidation kinetics during sintering using a phase field modeling based approach', Extreme Mechanics Letters, Vol. 7, pp.78-89.

[25] Panda, B.K. and Sahoo, S. (2018) 'Numerical simulation of residual stress in laser based additive manufacturing process', In IOP Conference Series: Materials Science and Engineering, Vol. 338, No. 1, p. 012030.

[26] Fang, Z.Z.sss ed. (2010) 'Sintering of advanced materials', Elsevier.